Boost-SEPIC Interleaved Converter with Integrated Magnetics

Juyeong Park and Honnyong Cha
School of Energy Engineering, Kyungpook National University, Daegu, Korea

***Abstract*-- This paper proposes an EE core structure coupled inductor with center gap design, which is applied in the Boost-SEPIC interleaved (BSI) converter. The proposed coupled inductor can integrate all three inductors with unequal voltage conditions. In addition, owing to the characteristics of the structure, each inductor current ripple is minimized, thus, the conduction loss is reduced, as well. Also, the overall size of the inductor is decreased significantly. The performance of the proposed coupled inductor is verified with a 2-kW prototype.**

***Index Terms*—Coupled inductor, current ripple reduction, DC-DC converter, step-up converter.**

I. Introduction

Recently, as environmental problems have been emerging, the demand for renewable energy such as fuel cells, PVs, and uninterrupted power supplies(UPS) has been increasing, as well [1]-[3]. Renewable energy system with low-voltage sources requires a step-up converter that converts low voltage into high voltage. To increase the voltage gain, many modified boost converter topologies have been investigated [4], [5]. In this article, the Boost-SEPIC interleaved (BSI) converter is introduced and analyzed in Fig. 1 [6], [7]. In the BSI converter, the average currents of each inductor are determined by the charge (amp-sec) balance condition of C_1 and C_2. The relationship between inductor currents is described in (1).

$$I_{L_1} = I_{L_2} + I_{L_3} \tag{1}$$

As a result, the BSI converter does not have a current balancing problem. The voltage gain can be shown as (1+D)/(1-D), which has a relatively high voltage gain compared to another non-isolated step-up converter. For the reason of this voltage gain, the input current becomes larger, so decreasing the current ripple is an important issue. An interleaving operation is an attractive method to reduce the ripple of input current. However, this method cannot reduce each inductor current ripple, which increases the conduction loss. This paper proposes an EE core structure coupled inductor with a center gap design that can reduce both the ripple of the input current and each inductor current [8]. The operation principle of the proposed coupled inductor is described. Also, the current ripple reduction effect of the coupled inductor compared to the conventional one is mathematically analyzed. In addition, this paper proposes a valid guideline for designing the coupled inductor. A 2-kW prototype was built with the fabricated inductor, and its performance was verified by the experimental waveform.

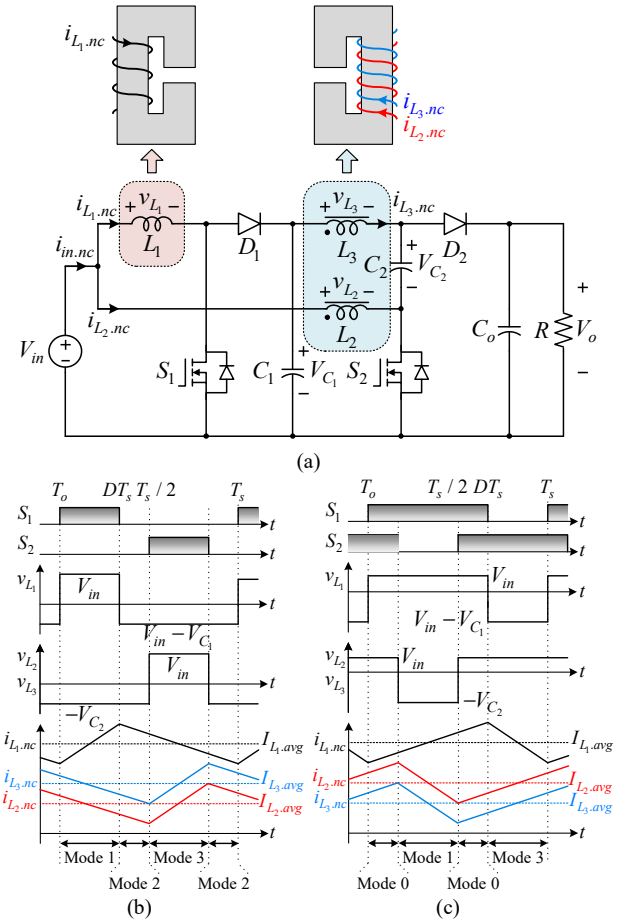

Fig. 1. Boost-SEPIC interleaved converter. (a) Topology, (b) Key waveforms with D≤0.5, (c) Key waveforms with D>0.5.

II. Principle of the Proposed Coupled Inductor

Conventional inductors can only be coupled when the waveforms of the voltages are the same. Therefore, L_2 and L_3 in the BSI converter can be integrated but it is impossible to integrate all three inductors in a single coupled inductor. The current waveforms of the non-coupled inductor case are described in Fig. 1(b) and Fig. 1(c) and the value of each inductor current ripple is expressed as (2). L_1, L_2, and L_3 are defined as self-inductance of inductors, respectively.

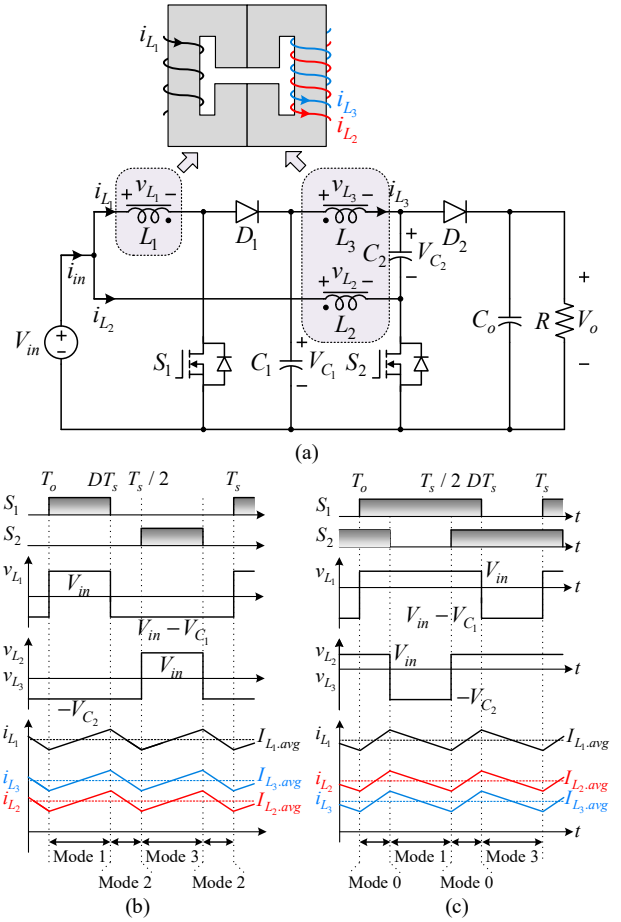

Fig. 2. BSI converter with the proposed coupled inductor. (a) Topology, (b) Key waveforms with D≤0.5, (c) Key waveforms with D>0.5.

$$\begin{cases} \Delta i_{L_1.nc} = \dfrac{V_{in} D T_s}{L_1} \\ \Delta i_{L_2.nc} = \dfrac{V_{in} D T_s}{2L_2} \\ \Delta i_{L_3.nc} = \dfrac{V_{in} D T_s}{2L_3} \end{cases} \tag{2}$$

However, all the inductors are integrated with the proposed structure, which lowers both the input current ripple and individual inductor current ripple. Furthermore, the size of the core decreases compared to the conventional inductors. The topology and the waveforms of the BSI converter with the proposed coupled inductor are shown in Fig. 2. The structure and operating principle of the proposed coupled inductor are shown in Fig. 3. An airgap is placed only in the center leg of the EE core, and windings are wound around the outer legs. The windings of L_2 and L_3 are wound together around the right-hand leg and winding of L_1 is inversely wound around the left-hand leg of EE core. N_1, N_2, and N_3 refer to the number of windings of each inductor.

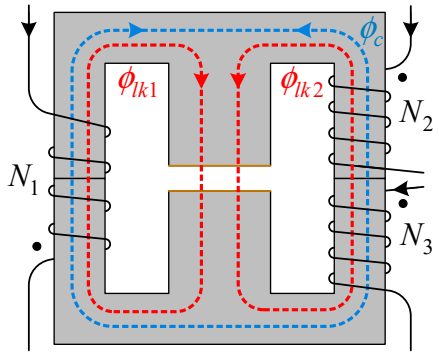

Fig. 3 Proposed coupled inductor structure.

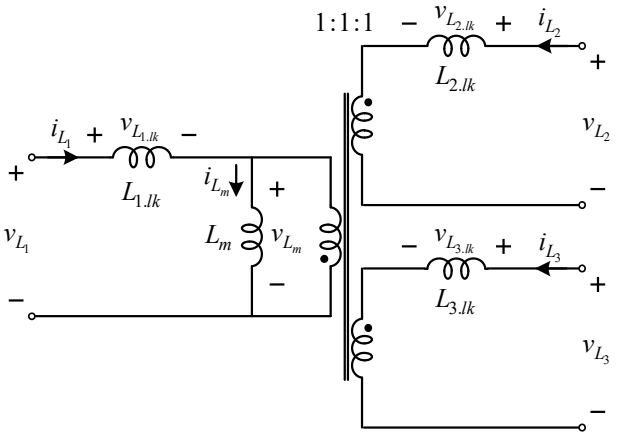

Fig. 4. Equivalent circuit model of the proposed coupled inductor.

A. Operation Principle of the Proposed Coupled Inductor

The flux generated by each winding can be functionally divided two types: coupling and leakage flux. Coupling flux (ϕ_c) flows through the outer path of the core and is presented as a blue dotted line in Fig. 3. It serves to transfer power like a transformer by inverse coupling between N_1, N_2 and between N_1, N_3. In Mode 1 and Mode 3, coupling flux is dominant and the slopes of the inductor current are changed from Fig. 1 to Fig. 2. As a result, the rising slope and falling slope of the inductor currents are presented two times in one switching period. In contrast, leakage fluxes(ϕ_{lk1}, ϕ_{lk2}) do not affect each other. In Fig. 3, they are presented by red dotted lines. Leakage fluxes are responsible for the leakage inductance in the circuit, which do not affect each other. Changing the length of the airgap in the center leg can adjust the leakage inductance value.

B. Derivation of Current Ripple Formula

The equivalent circuit model of the proposed coupled inductor is shown in Fig. 4. The leakage inductances are represented as $L_{1.lk}$, $L_{2.lk}$, $L_{3.lk}$, and magnetizing inductance is represented as L_m. The expression for the leakage inductance and magnetizing inductance is discussed in Section III. The voltage applied to L_m is reversely reflected to L_2 and L_3, and v_{L_1}, v_{L_2} and v_{L_3} can be shown as (3) with inversely coupled L_1, L_2, and L_1, L_3.

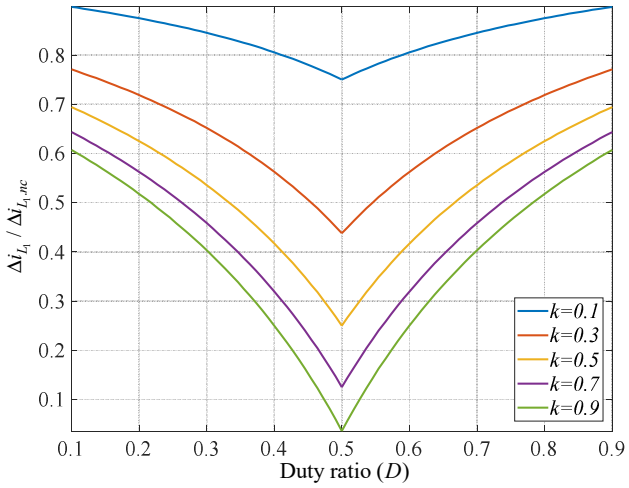

(a)

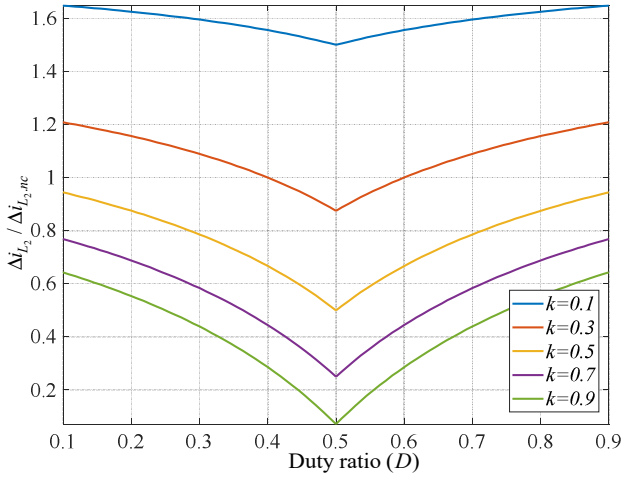

(b)

Fig. 5. Inductor current ripple ratio of coupled inductor with respect to the non-coupled case. (a) $\Delta i_{L_1}/\Delta i_{L_1.nc}$, (b) $\Delta i_{L_2}/\Delta i_{L_2.nc}$.

$$\begin{cases} v_{L_1} = v_{L_{1.lk}} + v_{L_m} = L_{1.lk}\dfrac{di_{L_1}}{dt} + L_m\dfrac{di_{L_m}}{dt} \\ v_{L_2} = v_{L_{2.lk}} - v_{L_m} = L_{2.lk}\dfrac{di_{L_2}}{dt} - L_m\dfrac{di_{L_m}}{dt} \\ v_{L_3} = v_{L_{3.lk}} - v_{L_m} = L_{3.lk}\dfrac{di_{L_3}}{dt} - L_m\dfrac{di_{L_m}}{dt} \end{cases} \tag{3}$$

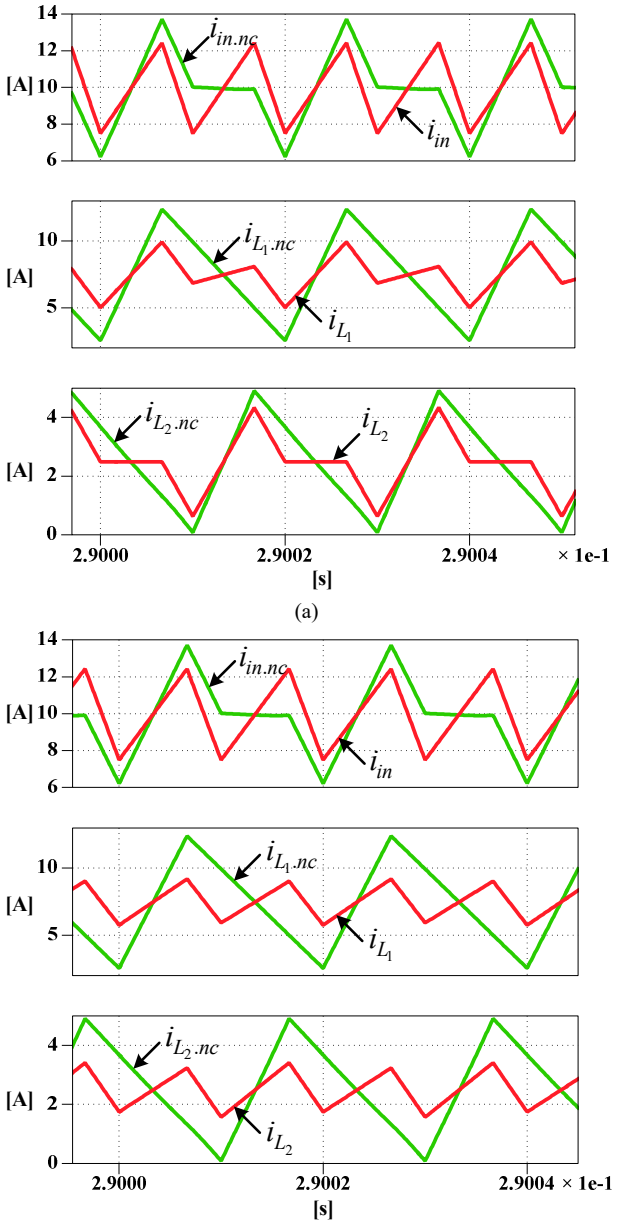

(a)

(b)

Fig. 6. Simulation results of input and inductor currents with the proposed coupled inductor. (a) k=0.5, (b) k=0.93.

1) $D \le 0.5$

$$\begin{cases} \Delta i_{L_1} = \dfrac{1}{L_{1.lk}}\dfrac{1+k-D-3kD}{(1+D)(1+2k)}V_o D T_s \\ \Delta i_{L_2} = \dfrac{1}{L_{2.lk}}\dfrac{1-D-kD}{(1+D)(1+2k)}V_o D T_s \\ \Delta i_{L_3} = \dfrac{1}{L_{3.lk}}\dfrac{1-D-kD}{(1+D)(1+2k)}V_o D T_s \end{cases} \tag{4}$$

2) $D > 0.5$

$$\begin{cases} \Delta i_{L_1} = \dfrac{1}{L_{1.lk}}\dfrac{-2k+D+3kD}{(1+D)(1+2k)}V_o (1-D) T_s \\ \Delta i_{L_2} = \dfrac{1}{L_{2.lk}}\dfrac{-k+D+kD}{(1+D)(1+2k)}V_o (1-D) T_s \\ \Delta i_{L_3} = \dfrac{1}{L_{3.lk}}\dfrac{-k+D+kD}{(1+D)(1+2k)}V_o (1-D) T_s \end{cases} \tag{5}$$

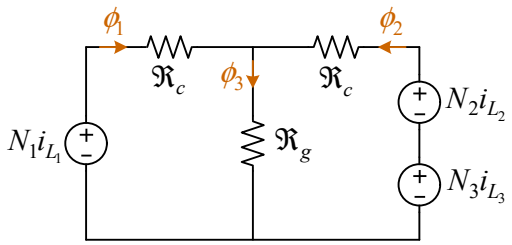

Fig. 7. Reluctance model of the proposed coupled inductor.

In (3), considering the flux balance condition, the following current ripple equation can be derived as (4) and (5). The current ripple can be derived with two conditions when $D \leq 0.5$ and $D > 0.5$. The current ripple of the inductors with D and coupling coefficient k is expressed in (4) and (5). The coupling coefficient between L_1 and L_2 (or L_3) is defined as k. In (4) and (5), the coupling coefficient between L_2 and L_3 is supposed to be one.

Fig. 5 shows the ratio of the inductor current ripple when using the proposed coupled inductor compared to the conventional inductors. In Fig. 5, it is assumed that the leakage inductance of the proposed coupled inductor and the self inductance of conventional inductance have the same value. In addition, it is assumed that both case have some switching period(T_s) and output voltage(V_o).

The ratio of the current ripple depends on k and D. As shown in Fig. 5, a higher k value significantly decreases the current ripple with proposed coupled inductor compared to the non-coupled inductor. Therefore, the k value should be designed close to one. It can be represented that the reduction of the inductor current ripple is also varying depending on the duty ratio. When the duty ratio is 0.5, the current ripple becomes smaller.

Fig. 6 shows the simulation results of the input currents and the inductor currents with $D = 0.33$. Fig. 6(a) is a comparison of non-coupled case and coupled case with $k = 0.5$, and Fig. 6(b) is a comparison of non-coupled case and coupled case with $k = 0.93$. The simulation results show that the ripple of input and inductor currents are smaller when using the proposed coupled inductor, but all the current ripple decreases more when the k value is sufficiently high. As shown in Fig. 6(a), the current ripple of the proposed coupled inductor is decreased about by 50 % with $k = 0.5$. In Fig. 6(b), it is decreased about by 35 % with $k = 0.93$, which shows the same results in Fig. 5.

III. Designs Guidelines for The Coupled Inductor

When designing more than two coupled inductors, additional considerations should be given than coupled inductors. In addition, the proposed inductor is different from the conventional core, so new guidelines are required.

A. Considering the Magnetomotive Force(MMF)

When winding multiple inductors around the core, it should be designed in consideration of MMF. Fig. 7 shows the reluctance model of the proposed coupled inductor. $\mathfrak{R}_c$ and $\mathfrak{R}_g$ represent reluctance of core and airgap, respectively.

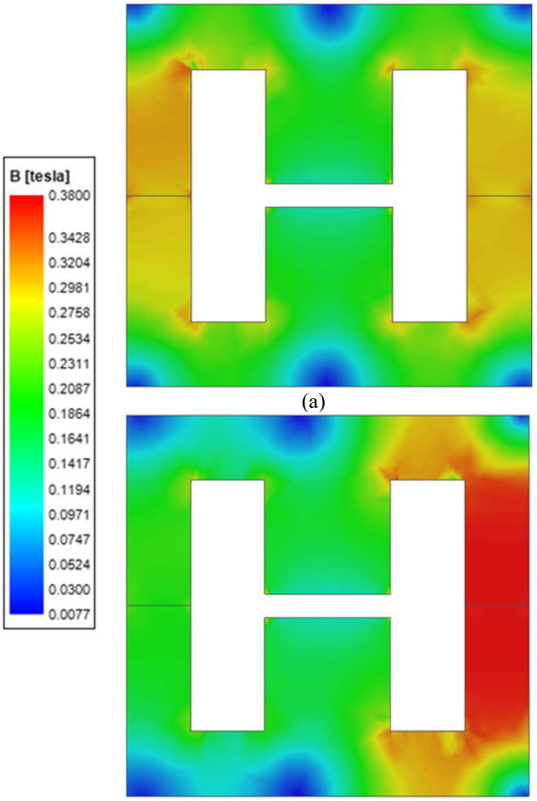

Fig. 8. Maxwell simulation results. (a) $N_1 = N_2 = N_3 = 20$, (b) $N_1 = 19$, $N_2 = N_3 = 20$.

$$\Phi \sum_k \mathfrak{R}_k = \sum_m N_m i_m \tag{6}$$

In magnetic circuits, (6) must be always satisfied by Ampere's law and continuity of flux[9]. The following equation is derived when (6) is applied to the reluctance model of Fig. 7. ϕ_1, ϕ_2, and ϕ_3 depict the fluxes that flow through each core leg.

$$N_1 i_{L_1} = N_2 i_{L_2} + N_3 i_{L_3} \tag{7}$$

If (7) is not satisfied, the core is saturated. Substituting the inductor current equation of (1) into (7) gives the condition for the number of turns of each inductor.

$$N_1 = N_2 = N_3 \tag{8}$$

Fig. 8 shows the results of ANSYS Maxwell software simulation and how the magnetic flux density changes when the MMF is different on the same core. Fig. 8(a) is designed to satisfy (8), so that all MMF values are the same. At this time, it can be confirmed that there is no saturated leg. However, in Fig. 8(b), the number of turns of the inductor L_1 is reduced by one turn. As a result, the right leg of the core is saturated.

B. Designing L_{lk} and k

Leakage inductance (L_{lk}) and coupling coefficient (k) are major factors that determine the current ripple of the

inductors as seen in (4) and (5). Therefore, when the proposed coupled inductor is fabricated, these two components must be correctly selected and designed. Since the structure is different from the conventional coupled inductor, this paper explains how to obtain the coupling coefficient between each inductor and the leakage inductance through the reluctance model[10].

The reluctance model of the proposed inductor is shown in Fig. 7. By applying (6), ϕ_1, ϕ_2, and ϕ_3 are calculated as follows;

$$\begin{cases} \phi_1 = \dfrac{\Re_c + \Re_g}{\Re_c(\Re_c + 2\Re_g)} N i_{L_1} - \dfrac{\Re_g}{\Re_c(\Re_c + 2\Re_g)} N(i_{L_2} + i_{L_3}) \\ \phi_2 = \dfrac{\Re_c + \Re_g}{\Re_c(\Re_c + 2\Re_g)} N(i_{L_2} + i_{L_3}) - \dfrac{\Re_g}{\Re_c(\Re_c + 2\Re_g)} N i_{L_1} \\ \phi_3 = \dfrac{1}{\Re_c + 2\Re_g} N(i_{L_1} + i_{L_2} + i_{L_3}) \end{cases} \quad (9)$$

By multiplying N and differentiating (9), the self-inductance (L_{self}) of each inductor and the magnetizing inductance can be obtained [10]. Also, leakage inductance and coupling coefficient can be calculated. As mentioned in Section II, this paper assumes that the coupling coefficient between L_2 and L_3 is one.

$$L_{self} = \frac{\Re_c + \Re_g}{\Re_c(\Re_c + 2\Re_g)} N^2 \quad (10)$$

$$L_m = \frac{\Re_g}{\Re_c(\Re_c + 2\Re_g)} N^2 \quad (11)$$

$$L_{lk} = L_{self} - L_m = \frac{N^2}{\Re_c + 2\Re_g} \quad (12)$$

$$k = \frac{L_m}{L_{self}} \quad (13)$$

C. Analysis of Flux Distribution

This paper obtains the instantaneous value of flux flowing in the leg inside the core. The maximum value of the magnetic flux obtained by adding the DC component and half of the ac component is shown in (14). The DC value of the magnetic flux is presented using the DC inductor currents, and the ac value is presented using the voltages on the inductors. In the case of $\phi_{3.m}$, since the ac value varies based on $D = 0.5$, the equation is divided into two cases.

$$\begin{cases} \phi_{1.m} = \dfrac{L_{lk}}{N} I_{L_1} + \dfrac{k}{1-k}\dfrac{L_{lk}}{N}(I_{L_1} - I_{L_2} - I_{L_3}) + \dfrac{V_{in} D T_s}{2N} \\ \phi_{2.m} = \dfrac{L_{lk}}{N}(I_{L_2} + I_{L_3}) + \dfrac{k}{1-k}\dfrac{L_{lk}}{N}(I_{L_2} + I_{L_3} - I_{L_1}) + \dfrac{V_{in} D T_s}{2N} \\ \phi_{3.m} = \begin{cases} \dfrac{L_{lk}}{N}(I_{L_1} + I_{L_2} + I_{L_3}) + \dfrac{V_{in}}{N}\dfrac{D\cdot(0.5-D)}{1-D} T_s, & D \le 0.5 \\ \dfrac{L_{lk}}{N}(I_{L_1} + I_{L_2} + I_{L_3}) + \dfrac{V_{in}}{N}(D-0.5) T_s, & D > 0.5 \end{cases} \end{cases} \quad (14)$$

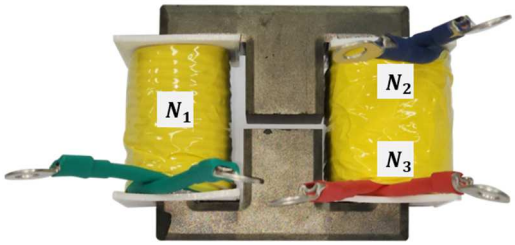

Fig. 9 Prototype photo of the proposed coupled inductor.

However, since (1) is satisfied in the BSI converter, (14) changed as follows.

$$\begin{cases} \phi_{1.m} = \dfrac{L_{lk}}{N} I_{L_1} + \dfrac{V_{in} D T_s}{2N} \\ \phi_{2.m} = \dfrac{L_{lk}}{N}(I_{L_2} + I_{L_3}) + \dfrac{V_{in} D T_s}{2N} \\ \phi_{3.m} = \begin{cases} \dfrac{L_{lk}}{N}(I_{L_1} + I_{L_2} + I_{L_3}) + \dfrac{V_{in}}{N}\dfrac{D\cdot(0.5-D)}{1-D} T_s, & D \le 0.5 \\ \dfrac{L_{lk}}{N}(I_{L_1} + I_{L_2} + I_{L_3}) + \dfrac{V_{in}}{N}(D-0.5) T_s, & D > 0.5 \end{cases} \end{cases} \quad (15)$$

Because the magnetic flux due to the difference DC value of the inductor current does not occur, unlike [10], the equation for the magnetic flux distribution is expressed regardless of k. Therefore, there is no need to reduce the k value to prevent saturation of the core.

IV. Experimental Results

Based on the guidelines obtained in Section III, a 2-kW prototype inductor is directly fabricated. Specifications of the inductor used in the experiment are shown in Table I, and the prototype of the proposed coupled inductor is shown in Fig. 9. In addition, the specifications used in the experiment are listed in Table II.

TABLE I
Specification of the Proposed Inductor

Core used	EE7066 (Ferrite core)
No. of turns	28
L_m	3.4 mH
L_{lk}	265 μH
Airgap	4 mm
k	0.928

TABLE II
Experimental Parameters

P_o	2 kW
f_{sw}	50 kHz
V_{in}, V_o	100 – 200 V, 400 V
D	0.33 – 0.6
Switch	IPW60R040C7
Diode	RHRG3060
C_1, C_2	40 μF
C_o	330 μF

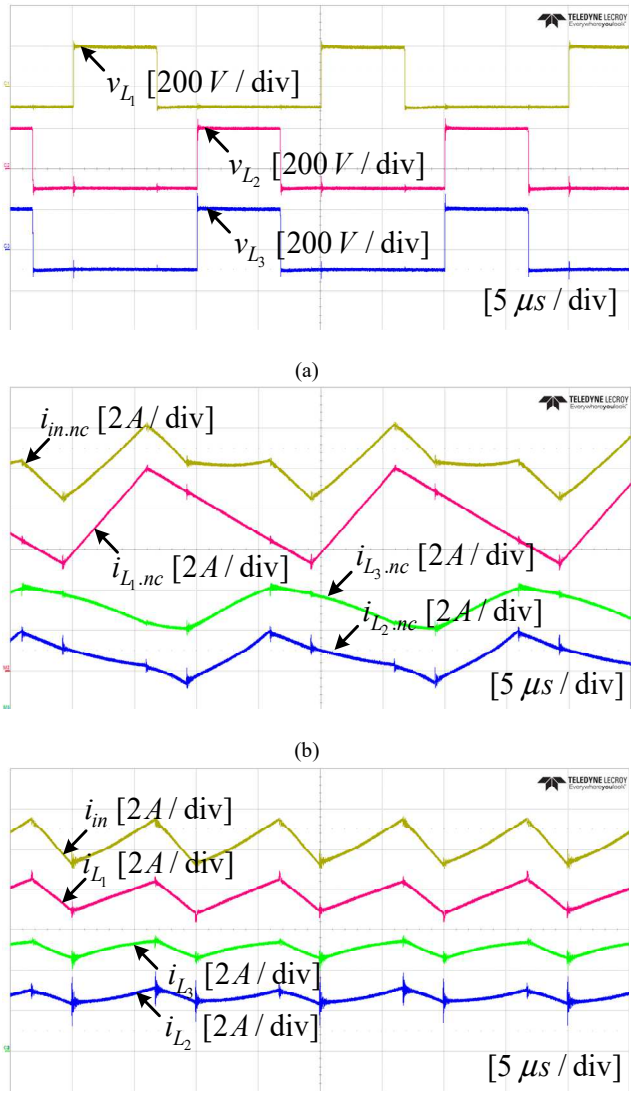

Fig. 10 Experimental waveforms when D=0.33. (a) Inductor voltage, (b) Inductor currents with L_2 and L_3 coupled, (c) Inductor currents with all inductors coupled.

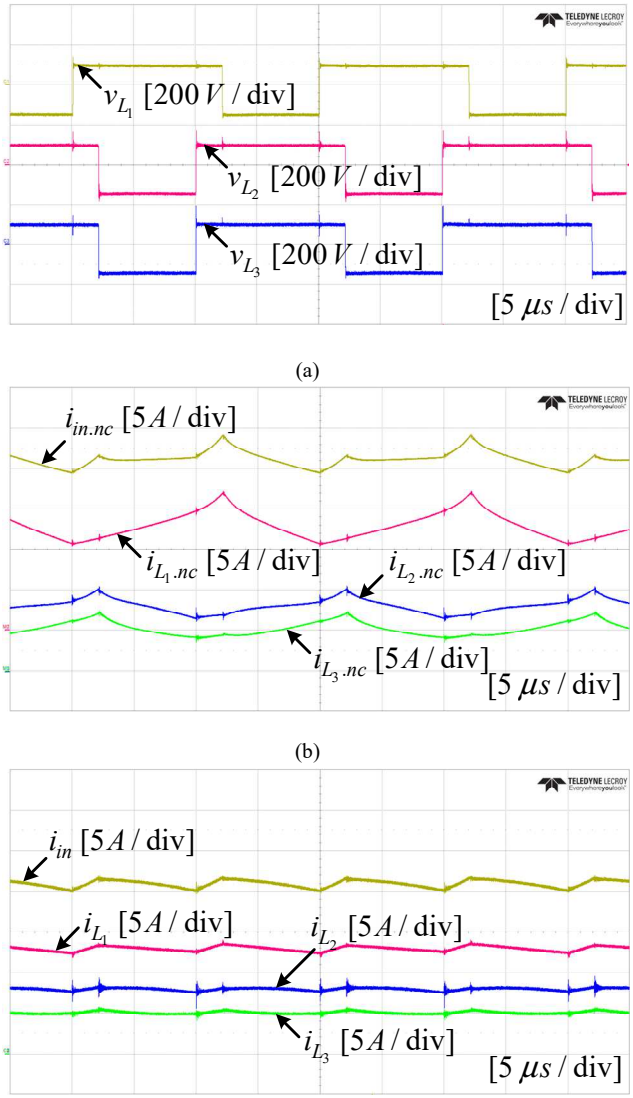

Fig. 11 Experimental waveforms when D=0.6. (a) Inductor voltage, (b) Inductor currents with L_2 and L_3 coupled, (c) Inductor currents with all inductors coupled.

Figs. 10 and 11 show the experimental results of the BSI converter when the duty ratio is 0.33 and 0.6, respectively. The voltage and current waveforms of the inductor are shown in Figs. 10 and 11. Compared to Fig. 10(b) and Fig. 10(c), the current ripple of L_1 with conventional inductor is 4.8 A, but with the proposed coupled inductor, it is reduced to about 1.6A by 33%. Also, Fig. 11(b) and Fig. 11(c) show that the current ripple decreases when the duty ratio is 0.33, which is less than 0.5. The current ripple of L_1 decreases from 6.8 A to 1.8 A by 26%. These results confirm the ratio of the current ripple depicted in Fig 5(a). Therefore, the performance of the proposed coupled inductor is verified.

V. Conclusion

This paper proposes the coupled inductor using the EE core structure with the center gap design that is applicable to the BSI converter. When both leakage inductance and coupling coefficient are large enough with the proposed coupled inductor, each inductor current ripple decreases and the size of the core can be decreased. This paper derived and proved the formula for the decrease of inductor current ripple. Also, guidelines for the design of EE core structure coupled inductor are introduced and verified with various simulations. A 2-kW prototype was built and verified by experiment.

Acknowledgment

This work was supported by the National Research Foundation of Korea(NRF) grant funded by the Korea government(MSIT) (NRF-2021R1A2C2007879).

References

[1] Haiping Xu, Li Kong and Xuhui Wen, "Fuel cell power system and high power DC-DC converter," *IEEE Trans. Power Electron.*, vol. 19, no. 5, pp. 1250-1255, Sept. 2004.

[2] R. Sharma and Hongwei Gao, "Low cost high efficiency DC-DC converter for fuel cell powered auxiliary power unit of a heavy vehicle," *IEEE Trans. Power Electron.*, vol. 21, no. 3, pp. 587-591, May 2006.
[3] H. Kakigano, Y. Miura and T. Ise, "Low-Voltage Bipolar-Type DC Microgrid for Super High Quality Distribution," *IEEE Trans. Power Electron*., vol. 25, no. 12, pp. 3066-3075, Dec. 2010.
[4] K. -B. Park, G. -W. Moon and M. -J. Youn, "Nonisolated High Step-up Boost Converter Integrated With Sepic Converter," *IEEE Trans. Power Electron.*, vol. 25, no. 9, pp. 2266-2275, Sept. 2010.
[5] H. Liu, H. Hu, H. Wu, Y. Xing and I. Batarseh, "Overview of High-Step-Up Coupled-Inductor Boost Converters," *IEEE J. Emerg. Sel. Top. Power Electron.*, vol. 4, no. 2, pp. 689-704, June 2016.
[6] Prajof P. and V. Agarwal, "Novel boost-SEPIC type interleaved dc-dc converter for low-voltage bipolar dc microgrid-tied solar pv applications," *2015 IEEE 42nd Photovoltaic Specialist Conference (PVSC)*, 2015, pp. 1-6.
[7] V. -C. Nguyen, H. Cha, D. -V. Bui and B. Choi, "Modified double-dual-boost high-conversion-ratio DC–DC converter with common ground and low-side gate driving," *IEEE Trans. Power Electron.*, vol. 37, no. 5, pp. 4952-4956, May 2022.
[8] Jong-Pil Lee, Honnyong Cha, Dongsul Shin, Kyoung-Jun Lee, Dong-Wook Yoo, Ji-Yoon Yoo, “Analysis and design of coupled inductors for two-phase interleaved DC-DC converters,” *JOURNAL OF POWER ELECTRONICS*, 13(3), 339-348, 2013.
[9] Mohan, Ned, Tore M. Undeland, and William P. Robbins, “Review of Basic Electrical and Magnetic Circuit Concepts,” *Power electronics: converters, applications, and design*., John wiley & sons, 2003, pp. 33-60.
[10] A. Pietkiewicz and D. Tollik, "Coupled-inductor current-doubler topology in phase-shifted full-bridge DC-DC converter," INTELEC - Twentieth International Telecommunications Energy Conference San Francisco, CA, USA, 1998, pp. 41-48.